# Vibronic Spectra of $\pi$ -Conjugated Systems with a Multitude of Coupled States. A Protocol Based on Linear Vibronic Coupling Models and Quantum Dynamics Tested on Hexahelicene

Daniel Aranda and Fabrizio Santoro*

*CNR–Consiglio Nazionale delle Ricerche, Istituto di Chimica dei Composti Organo Metallici (ICCOM-CNR), SS di Pisa, Area della Ricerca, via G. Moruzzi 1, I-56124 Pisa, Italy*

E-mail: fabrizio.santoro@pi.iccom.cnr.it

## Abstract

Hexahelicene is a prototype of an extended $\pi$-conjugated system with axial chirality. Its absorption (ABS) and electronic circular dichroism spectra (ECD) show vibronic features and strong nonadiabatic effects, challenging currently available computational methods. Here we compute the nonadiabatic ABS and ECD vibronic spectra of hexahelicene in the full energy range, covering $\sim 2$ eV and 14-18 coupled electronic states, including all the relevant nuclear coordinates. To this end we exploit a recently-proposed protocol that uses time-dependent density functional theory to parametrize Linear Vibronic Coupling models comprising several electronic states. Spectra are computed through quantum dynamical propagations with multiconfigurational time-dependent Hartree methods. Our results nicely reproduce the experimental spectra providing an assignment of the main observed bands. On the contrary, we document that application of Herzberg-Teller intensity-borrowing theory leads to large artefacts. The proposed approach is of general applicability for rigid systems and represents a viable tool for studying the photophysical properties of $\pi$-conjugated systems characterized by a dense manifold of interacting electronic states.

# 1 Introduction

Photophysical properties of molecules with extended $\pi$-conjugation are of paramount importance in material science. These systems are usually characterized by a dense manifold of electronic states so that significant inter-state couplings, mediated by vibrational modes, are expected. The calculation of the lineshape of molecular electronic spectra has known great progress in the last decades, and nowadays effective time-independent [1–6] (TI) and time-dependent [7–12] (TD) vibronic approaches are available. However they are "adiabatic", in the sense that they assume inter-state couplings are negligible or very weak. Therefore they are not suitable in principle to deal with molecules with dense manifolds of states. This contribution shows that, if a $\pi$-conjugated system is rigid, a proper computation of its nonadiabatic vibronic spectrum is now at hand through wavepacket quantum dynamical (QD) propagations on coupled diabatic potential energy surfaces (PES). This result is achieved combining the impressive progresses in the multiconfigurational time-dependent Hartree method (MCTDH), [13,14] and its multilayer extension, [15–17] with an effective and automatic method we have recently proposed [18] for the generation of linear vibronic coupling (LVC) models for several excited states. [19,20] It exploits a maximum-overlap diabatization technique and parametrize the LVC with respect to time-dependent density functional theory (TD-DFT) calculations. [18]

Helicenes are polycyclic aromatic compounds, in which benzenes or other aromatics are ortho-fused to impart a chiral helical structure. [21,22] They are the prototype of systems with axial chirality and are actively explored as building blocks for new materials with unprecedented chiroptical properties. [23,24] Theoretical models and computational methods have proven to be very helpful in the interpretation of the chiroptic properties of both single molecules, [25,26] and supramolecular aggregates, thanks to the efforts born with the well know exciton chirality method. [27–29] However, the computation of the vibronic spectra of helicenes still constitute a challenge. In fact even a member of the series with moderate length like hexahelicene, made up by 6 fused benzenes ([6]helicene), exhibits an electronic spectrum covering $\sim$ 2 eV with contributions (depending on the electronic method) from 14 up to 18 electronic states. Due to their average spacing ($< 0.15$ eV) a single quantum on a collective C-C stretching vibrational mode, like those typically activated during electronic excitation, is expected to create resonances and therefore mixing of vibronic states.

Here we show that a LVC model parametrized with respect to TD-DFT, in combination with ML-MCTDH propagations including all relevant normal coordinates, allows to reproduce the experimental absorption (ABS) and Electronic Circular Dichroism (ECD) spectra of [6]helicene in the full frequency range, and a confident assignment of the main bands. At the same time we document that adiabatic vibronic approaches fail to reproduce several features of the spectra. In particular, application of Herzberg and Teller (HT) [30] approach, routinely adopted to describe intensity-borrowing of weak bands due to the coupling with strong transitions, cannot explain the existence of some bands and, what is worse, introduces large artefacts on the intensities of the spectra. Both problems are intrinsically due to the limitations of HT perturbative approach. Similar problems of adiabatic methods have been encountered recently for other achiral [31] and chiral structures with large $\pi$-systems, [32,33] and are actually expected to be quite general for systems with extended $\pi$-conjugation.

# 2 Methods

## 2.1 Theory

We consider a set of coupled electronic diabatic states $d_i$ and a LVC Hamiltonian in the dimensionless normal coordinates $\mathbf{q}$ (and associated momenta $\mathbf{p}$) of the ground state ($g$),

$$\begin{aligned}\mathbf{H} &= \sum_i \Big(K + V_{ii}^{dia}(\mathbf{q})\Big) |d_i\rangle \langle d_i| \\ &\quad + \sum_{i,j>i} V_{ij}^{dia}(\mathbf{q}) \Big( |d_i\rangle \langle d_j| + |d_j\rangle \langle d_i| \Big) \quad (1)\end{aligned}$$

The kinetic ($K$) and potential ($V$) terms are

$$K = \frac{1}{2}\mathbf{p}^T \mathbf{\Omega} \mathbf{p} \quad (2)$$

$$V_{ii}^{dia}(\mathbf{q}) = E_i^0 + \boldsymbol{\lambda}_{ii}^T \mathbf{q} + \frac{1}{2}\mathbf{q}^T \mathbf{\Omega} \mathbf{q}, \quad (3)$$

$$V_{ij}^{dia}(\mathbf{q}) = \boldsymbol{\lambda}_{ij}^T \mathbf{q}. \quad (4)$$

where $\mathbf{\Omega}$ is the diagonal matrix of the vibrational frequencies of state $g$. $E_i^0$ is the $i$th excited-state energy at the $g$ equilibrium geometry, $\boldsymbol{\lambda_{ii}}$ is the energy gradient of state $i$ and accounts for a shift of the equilibrium position and $\boldsymbol{\lambda_{ij}}$ is the gradient of the inter-state coupling $V_{ij}^{dia}(\mathbf{q})$. Therefore $V_{ii}^{dia}(\mathbf{q})$, the PES of diabatic state $i$, is a quadratic function of $\mathbf{q}$ that shares the same normal modes and frequencies of $g$ and the inter-state couplings $V_{ij}^{dia}(\mathbf{q})$ are linear functions of $\mathbf{q}$.

In a TD framework the ABS $\epsilon(\omega)$ and ECD $\Delta\epsilon(\omega)$ spectra (at 0 Kelvin) can be written as

$$\begin{aligned}\frac{\epsilon(\omega)}{\mathcal{C}_\epsilon} &= \omega \sum_{ji} \int_{-\infty}^{\infty} dt e^{i\omega t - \Gamma t^2} \langle \mathbf{0}; d_j | \boldsymbol{\mu}_{gj} e^{-i\mathbf{H}t/\hbar} \boldsymbol{\mu}_{ig} | d_i; \mathbf{0} \rangle \\ &= \sum_i \epsilon_{ii}(\omega) + \sum_{i,j\neq i} \epsilon_{ij}(\omega) \quad (5)\end{aligned}$$

$$\begin{aligned}\frac{\Delta\epsilon(\omega)}{\mathcal{C}_{\Delta\epsilon}} &= \omega \sum_{ji} \int_{-\infty}^{\infty} dt e^{i\omega t - \Gamma t^2} \langle \mathbf{0}; d_j | \boldsymbol{m}_{gj} e^{-i\mathbf{H}t/\hbar} \boldsymbol{\mu}_{ig} | d_i; \mathbf{0} \rangle \\ &= \sum_i \Delta\epsilon_{ii}(\omega) + \sum_{i,j\neq i} \Delta\epsilon_{ij}(\omega) \quad (6)\end{aligned}$$

where $\mathcal{C}_\epsilon$ and $\mathcal{C}_{\Delta\epsilon}$ collect physical constants specified in the SI and we introduced a quadratic damping ruled by a parameter $\Gamma$, corresponding to a Gaussian broadening in the frequency domain. $\boldsymbol{\mu}_{gj} = \langle g|\boldsymbol{\mu}|d_j\rangle$ and $\boldsymbol{m}_{gj} = Im[\langle g|\boldsymbol{m}|d_j\rangle]$, are respectively the so called electric and magnetic transition dipole moments, and $\mathbf{0}$ is the ground-vibrational state of the ground electronic state (whose energy is set to 0). Practically, in order to perform the calculations, we propagate in time under the effect of the LVC Hamiltonian each doorway state $|d_j;\mathbf{0}\rangle$ obtained by a vertical excitation to state $j$. This allows us to compute the auto- ($i = j$) and cross- ($i \neq j$) correlation functions in the integrals in Eqs. 5 and 6. The latter functions are then summed with weights equal to the corresponding scalar products of the electric transition dipoles (ABS), or of the electric and magnetic transition dipoles (ECD). As a last step, the vibronic spectra are obtained by Fourier transform. These spectra are "nonadiabatic", in the sense that they explicitly account for inter-state couplings which affect both the diagonal contributions ($\epsilon_{ii}(\omega)$ and $\Delta\epsilon_{ii}(\omega)$) and the off-diagonal ones ($\epsilon_{ij}(\omega)$ and $\Delta\epsilon_{ij}(\omega)$). In the SI we connect Eqs 5 and 6 to the more popular TI sum-over-states expressions.

LVC can be viewed as a generalization of the adiabatic approach known as Vertical Gradient (VG).[34] Like LVC, VG assumes that excited-states normal modes and frequencies are equal to those of the ground state but it neglects inter-state couplings. In LVC model we use diabatic states, defined so to be ideally independent of the nuclear coordinates; therefore the vectors $\boldsymbol{\mu}_{jg}$ and $\boldsymbol{m}_{jg}$ can be considered constant, an approximation known as Condon or Franck-Condon (FC). On the contrary, adiabatic states change with coordinates and the dependence on $\mathbf{q}$ of transition dipoles can be expressed with a Taylor expansion:

$$\boldsymbol{\mu}_{jg}^{ad,LVC}(\mathbf{q}) = \boldsymbol{\mu}_{jg}^{FC} + \sum_\alpha \left(\frac{\partial \boldsymbol{\mu}_{jg}^{ad,LVC}(\mathbf{q})}{\partial q_\alpha}\right)_{FC} q_\alpha + \cdots \quad (7)$$

$$\boldsymbol{m}_{jg}^{ad,LVC}(\mathbf{q}) = \boldsymbol{m}_{jg}^{FC} + \sum_\alpha \left(\frac{\partial \boldsymbol{m}_{jg}^{ad,LVC}(\mathbf{q})}{\partial q_\alpha}\right)_{FC} q_\alpha + \cdot\cdot \quad (8)$$

Accounting only for the constant term, computed at the FC position, $\boldsymbol{\mu}_{jg}^{FC}$ and $\boldsymbol{m}_{jg}^{FC}$, leads to the model known as FC|VG, while considering also the linear terms one uses the so called HT approximation;[30] spectra that sum the FC and HT terms will be named FCHT|VG.

Obtaining the adiabatic states by diagonalization of the LVC Hamiltonian matrix, one can show that the energy gradients of the adiabatic states of the VG model and the energy-gradients of the LVC diabatic PES $V_{ii}$ coincide. Moreover, first-derivatives of the adiabatic transition dipoles are easily obtained.[35]

This procedure reflects the fact that the linear dependence on $\mathbf{q}$ of the transition dipoles arises from the existence of the inter-state couplings (see SI). Such a connection was exploited by HT, who proposed to use these linear terms to introduce the intensity-borrowing effect due to inter-state couplings in "adiabatic" approaches.

Eqs. 5 and 6 hold of course also for FC|VG and FCHT|VG models, but in this case $d$ shall be interpreted as adiabatic states. It is readily seen that since VG model neglects inter-state couplings, FC|VG and FCHT|VG spectra can be computed as the sum of the independent contributions of each adiabatic state. In particular only auto-correlation functions are different from zero and, since they describe the wavepacket motion on harmonic PES they can be computed analytically.[7–12]

The calculation of the spectra can be further simplified by totally neglecting the effect of vibrational motion, i.e. setting the correlation functions in Eqs. 5 and 6 to 1. In that case we obtain what is usually known as a purely-electronic spectrum where any vibronic information is lost and the contribution of each electronic state $i$ is simply a Gaussian whose integral for ABS and ECD is proportional respectively to the dipole ($D_{gi}^{FC} = |\boldsymbol{\mu}_{gi}^{FC}|^2$) or rotatory ($R_{gi}^{FC} = \boldsymbol{m}_{gi}^{FC}\boldsymbol{\mu}_{ig}^{FC}$) strength.

Analytical expressions for the total intensities can be straightforwardly obtained considering ABS and ECD lineshapes, $\epsilon(\omega)/\omega$ and $\Delta\epsilon(\omega)/\omega$, neglecting the prefactors $\mathcal{C}_\epsilon$ and $\mathcal{C}_{\Delta\epsilon}$, and integrating over the frequency.

$$I_{ABS} = \sum_i \langle \mathbf{0}|\boldsymbol{\mu}_{gi}\boldsymbol{\mu}_{ig}|\mathbf{0}\rangle \quad (9)$$

$$I_{ECD} = \sum_i \langle \mathbf{0}|\boldsymbol{m}_{gi}\boldsymbol{\mu}_{ig}|\mathbf{0}\rangle \quad (10)$$

Since in the LVC case the electronic transition dipoles are independent of the coordinates, they can be taken out of the brackets and we simply obtain

$$I_{ABS}^{LVC} = \sum_i |\boldsymbol{\mu}_{gi}^{FC}|^2 = \sum_i D_{gi}^{FC} \quad (11)$$

$$I_{ECD}^{LVC} = \sum_i \boldsymbol{m}_{gi}^{FC}\boldsymbol{\mu}_{ig}^{FC} = \sum_i R_{gi}^{FC} \quad (12)$$

This means that for absorption (ECD), total intensities are equal respectively to the sum of the dipole (rotatory) strengths $D_{gi}^{FC}(R_{gi}^{FC})$ from the ground state $g$ to all the considered excited states $i$. This is clearly the same result one would obtain for a purely-electronic calculation. For an adiabatic FC|VG calculation, the electronic transition dipoles are taken to be equal only to the constant term in the rhs of Eqs. 7 and 8.

Therefore, also in this case we have

$$I_{ABS}^{FC} = I_{ABS}^{LVC} = \sum_i |\boldsymbol{\mu}_{gi}^{FC}|^2 = \sum_i D_{gi}^{FC} \quad (13)$$

$$I_{ECD}^{FC} = I_{ECD}^{LVC} = \sum_i \boldsymbol{m}_{gi}^{FC} \boldsymbol{\mu}_{ig}^{FC} = \sum_i R_{gi}^{FC} \quad (14)$$

On the contrary, for an adiabatic FCHT calculation both the terms in the rhs of Eqs. 7 and 8 must be considered. The integrals can be quickly evaluated in second quantization $q_\alpha = 1/\sqrt{2}(a_\alpha + a_\alpha^+)$ obtaining

$$\begin{aligned} I_{ABS}^{FCHT} &= I_{ABS}^{FC} + \frac{1}{2}\sum_{i\alpha}\left[\left(\frac{\partial \boldsymbol{\mu}_{gi}^{ad,LVC}(\mathbf{q})}{\partial q_\alpha}\right)_{FC}\right]^2 \\ &= \sum_i (I_{ABS,i}^{FC} + I_{ABS,i}^{HT}) \quad (15) \\ I_{ECD}^{FCHT} &= I_{ECD}^{FC} + \\ &\quad \frac{1}{2}\sum_{i\alpha}\left(\frac{\partial \boldsymbol{m}_{gi}^{ad,LVC}(\mathbf{q})}{\partial q_\alpha}\right)_{FC}\left(\frac{\partial \boldsymbol{\mu}_{ig}^{ad,LVC}(\mathbf{q})}{\partial q_\alpha}\right)_{FC} \\ &= \sum_i (I_{ECD,i}^{FC} + I_{ECD,i}^{HT}) \quad (16) \end{aligned}$$

Therefore at FCHT level the total intensities are not equal to the FC and LVC cases, since each state contributes with two terms: the FC one and a second one (HT) which depends on the transition dipoles derivative. Notice that for absorption the HT terms is always positive, therefore $I_{ABS}^{FCHT} \geq I_{ABS}^{FC}$.

### 2.2 Computational Details

Here we report calculations in gas-phase with TD-DFT, adopting mainly the M06-2X functional in combination with the 6-31G(d) basis set. Convergence tests were performed with the more extended 6-311+G(2d,2p) basis set, and some spectra have been computed also with B3LYP and CAM-B3LYP functionals including Grimme's dispersion corrections with Becke-Johnson damping (GD3BJ).[36] In the literature, accurate coupled cluster methods have also been employed at pure-electronic level for [6]helicene with very good results,[37] however the computational cost would make the parametrization of the LVC Hamiltonian unfeasible. All electronic calculations were run with Gaussian 16.[38] The LVC Hamiltonian was parametrized on the grounds of a maximum-overlap diabatization, with a house made code, available upon request, interfaced with Gaussian package.[18] Details on the diabatization protocol are given in Section S1 of the SI. In practice, in a first step, adiabatic states at the ground state equilibrium geometry are computed and taken as a reference to define the diabatic states. Then, the molecular structure is displaced along all normal modes, and at each new geometry diabatic states are defined as the rotation of the adiabatic states that resemble as much as possible the reference states. Therefore, as far as electronic computations are concerned, the cost is equivalent to the one for the calculation of numerical gradients for all the involved states, plus the computation of the overlaps between transition densities at displaced geometries (performed by our code). Once obtained the LVC parameters, MCTDH and ML-MCTDH wavepacket propagations were run with the Quantics code,[39,40] with the specific settings described in the SI. We included the 14 (18 for B3LYP) lowest-energy diabatic states and all the normal coordinates $\alpha$ (63 out of 120, 65 for B3LYP) for which the absolute value of any of the $\lambda_{ij}(\alpha)$ coupling constants is larger than 0.02 eV. Increasing the threshold to 0.03 eV reduces the number of normal modes to 40 (CAM-B3LYP) without appreciable changes in the spectra (see Sction S3.2 of the SI). The normal coordinates were combined as shown in the ML-MCTDH tree in Figures S4, S8 and S9 for M06-2X, CAM-B3LYP and B3LYP parametrizations, respectively. To improve the reproduction of the weak bands in the 3.0-3.3 eV region discussed in Section 3.2.3, the number of single particle and primitive functions was increased as reported in Figure S7. Convergence of the spectra was checked with respect to the number of coordinates, single particle functions and the dimension of the primitive basis set in Section S3.2 of the SI. FC|VG and FCHT|VG adiabatic spectra (including the effect of all the 120 vibrational coordinates) have been computed with our code *FCclasses* 3.0,[41] from analytical TD correlation functions,[12] or with effective TI pre-screening methods which make easier the assignments in terms of vibrational quantum numbers.[3,4]

## 3 Results and Discussion

### 3.1 Electronic Spectra

Figure 1 compares purely-electronic ABS and ECD spectra of (*M*)-[6]helicene with experiments in chloroform.[42] Computations were performed in gas phase for the first 20 states with the 6-31G(d) and 6-311+G(2d,2p) basis sets (see Table S1 for details). The shape of the spectra with the two bases is similar, in particular up to 4.5 eV (exp. values). Since electronic spectra miss vibronic details, which are however observed in the experiment, it is not possible to establish a one-to-one correspondence between computed and experimental peaks and so estimate an "error" in the computed vertical excitations. In Figure 1 we approximately matched the computed lowest-energy strong ABS peak (due to state S3) with the two experimental peaks at 3.9-4.0 eV. This suggests a blue-shift of 0.30 and 0.20 eV for the calculations with 6-31G(d) and 6-311+G(2d,2p), respectively. Figure 1 also suggests that the error is larger by an additional ∼0.2-0.25 eV for the bands above 4.5 eV. In any case the first 14 electronic states appear sufficient to simulate the energy range covered by experiments. Notice that the experimental band at ∼3.5-3.6 eV is missing in the computations and that, on the other hand, the computed ECD band at 4.20 eV in Figure 1, due to state S6, seems not to have an experimental counterpart. As discussed later, the ex-

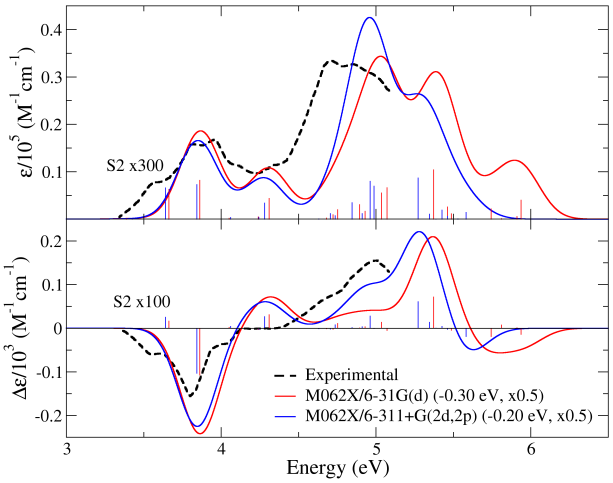


**Figure 1:** ABS (top) and ECD (bottom) spectra of (*M*)-[6]helicene calculated at pure-electronic level with M062X/6-31G(d) and M062X/6-311+G(2d,2p), shifted and scaled as shown in the legends, are compared to experiment. All stick transitions were convoluted with a Gaussian with HWHM = 0.15 eV. Notice that the intensity of S2 stick bands has been amplified to make them visible.

perimental spectra exhibit also an extremely weak progression of bands with an onset at 3.0 eV, which arises from the contribution of S1 and cannot be appreciated with the scale of Figure 1. Their intensities are better reproduced with the 6-311+G(2d,2p) basis set.

Therefore in the following we report vibronic calculations for the first 14 states on the grounds of PES parametrized with the more convenient 6-31G(d) basis set, but we correct the transition dipoles with the 6-311+G(2d,2p) basis set. For comparison, results obtained with the 6-31G(d) transition dipoles are given in Figure S2 of the SI.

## 3.2 Vibronic Spectra

We start analysing the performance of the adiabatic FC|VG approach. Sketches of the most relevant normal modes for the following analysis are given in Figure S13 of the SI. The two central panels of Figure 2 compares FC|VG spectra with experiment for ABS (panel b) and ECD (panel c). Panels a (ABS) and d (ECD) of the same Figure reports the contribution of each of the 14 electronic states with the assignments of the main bands. Interestingly, besides the contribution of low-frequency modes which only introduce a broadening, the vibronic structure of most of these spectra is similar and essentially due to a progression along mode v85, a totally symmetric ring deformation with frequency ∼1400 $cm^{-1}$. Up to 4.5 eV, FC|VG remarkably improves over the purely-electronic results in Figure 1. The error on the position is reduced from ∼ 0.3 to ∼ 0.21 eV, and the modulation of the experimental ABS intensity between 3.8 and 4.0 eV is now explained by a vibronic progression along mode v85 on state S3. Furthermore, it emerges that the spurious ECD band at 4.2 eV, was

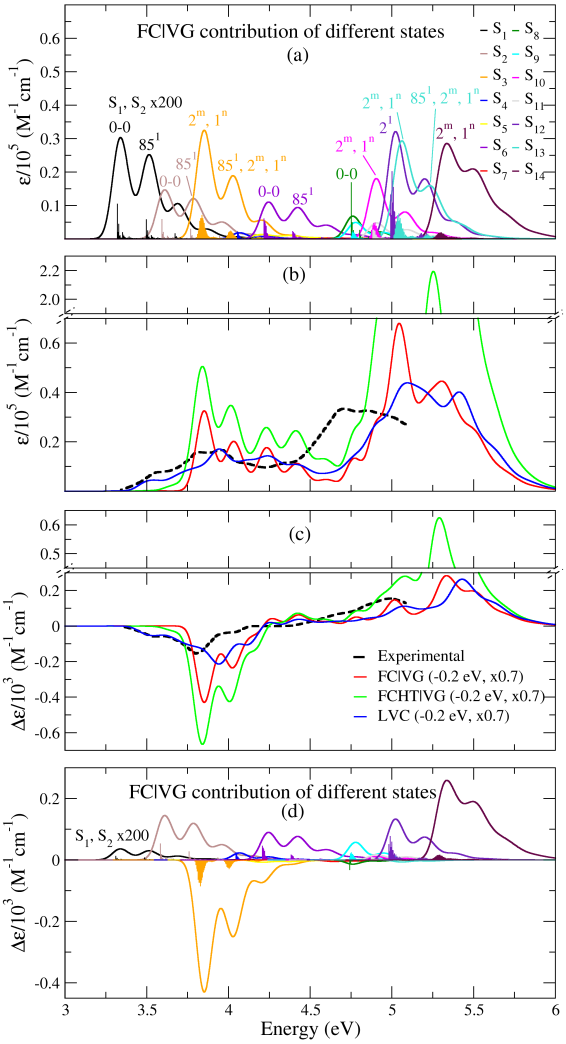


**Figure 2:** Comparison of (*M*)-[6]helicene experimental ABS (b) and ECD (c) spectra with the predictions of FC|VG, FCHT|VG and LVC (including 63 coordinates and only the auto-correlation terms in Eqs.5,6). Calculated spectra were redshifted by 0.2 eV and scaled by a factor of 0.7. All stick transitions were convoluted with a Gaussian of HWHM = 0.05 eV. Panels (a) and (d) show the FC|VG contribution of each state and the vibronic stick transitions for ABS and ECD, respectively; S1 and S2 intensity were increased by a factor of 200. Assignments $m^n$ in terms of modes $m$ and quanta $n$ are given in panel (a) for the most intense vibronic transitions.

not due to an inaccuracy in the electronic calculations. In fact, once vibronic contributions are included, the band is erased by the compensation between the bands of S3 and S6 (see panel d). Despite these improvements, FC|VG calculations cannot explain the experimental band at ∼3.5-3.6 eV.

We then apply the LVC model in combination with ML-MCTDH propagations. In Figure S17 of the SI we show that the contribution of off-diagonal terms in Eqs. 5 and 6 ($i \neq j$) is very small so it will be neglected in the following. Figure 2b and 2c show that LVC successfully reproduce the missing ABS and ECD band at ∼3.5-3.6 eV. Its origin is investigated below. As far as the other portions of the spectrum are concerned, LVC significantly improves over FC|VG up to < 4.5 eV, since

**Table 1:** $I^{FC}_{ABS}$, $I^{HT}_{ABS}$, $I^{FCHT}_{ABS}$ absorption intensities (in atomic units) for S2, S3 and S10-S13 excited states.

| | ABS Intensity (a.u.) | | |
|---|---|---|---|
| State | $I^{FC}_{ABS}$ | $I^{HT}_{ABS}$ | $I^{FCHT}_{ABS}$ |
| S2($A$) | 0.01 | 3.31 | 3.32 |
| S3($B$) | 3.70 | 0.07 | 3.77 |
| Total Intensity | 3.71 | 3.38 | 7.09 |
| S10($A$) | 1.45 | 2.37 | 3.82 |
| S11($B$) | 0.46 | 4.56 | 5.02 |
| S12($A$) | 2.98 | 6.46 | 9.44 |
| S13($B$) | 3.42 | 8.75 | 11.52 |
| Total Intensity | 7.66 | 22.14 | 29.80 |

it better reproduces the smoothing of the vibronic structures observed in the experiment. The comparison at energies $> 4.5$ eV is postponed to Section 3.3.

### 3.2.1 Failure of the FCHT approximation above 3.5 eV

As we discussed above, intensity-borrowing due to inter-state couplings can be, in principle, described also with the adiabatic FCHT|VG approach. FCHT|VG has been very successful and its application is straightforward.[4,9–11] Focusing on ECD, FCHT approximation has been able to reproduce and explain weak bisignated ECD spectra of single electronic states, sometimes described as "forbidden-character" of ECD.[43–47]

However, for [6]helicene Figure 2b and 2c document a spectacular failure of the FCHT|VG approach for both ABS and ECD spectra. On one side FCHT|VG is not able to reproduce the band at ∼3.5-3.6 eV, correctly described by LVC, on the other side it predicts spectra very similar to the FC|VG in shape but by far more intense, remarkably worsening the agreement with experiments. Notice, in fact, the breaks along the $y$ axis in the central panels of Figure 2 (full-range figures are given in Figure S16). Both problems are intrinsically connected with the perturbative HT approach. On one side, in VG model vibrational states and energies are assumed to not be affected by the inter-state couplings. On the other side, there is a fundamental problem with the intensity predicted by FCHT.

As we showed in Eqs. 13-16, the equivalent of FC and LVC total intensities indicate that inter-state couplings can redistribute the intensity of the spectrum lineshape but do not alter its integral. On the contrary, FCHT predicts that the total intensity of the spectrum deviates from the FC case and depends on the derivatives of the transition dipoles with respect to the normal coordinates.

The issue with the intensity is better explained focusing on ABS because, as noticed above, by construction $I^{FCHT}_{ABS} \geq I^{FC}_{ABS}$. Table 1 reports the largest values of $I^{HT}_{ABS}$ which are predicted for states S2 and S10-S13. Also S3 values are given since S2 acquires intensity through the coupling with S3. Equivalent data for other states can be found in Section S3.4 of the SI. The sum of the $I^{FCHT}_{ABS}$ for S2-S3 and S10-S13 is respectively two and three times larger than $I^{FC}_{ABS}$. For ECD the problem is less evident because of the mutual cancellation of intensities but it clearly exists (Table S4).

Inspection of the contribution of the different normal modes shows that $I^{HT}_{ABS}$ mainly originates from 4 normal modes (v97, v99, v102 and v104, see Table 2). They are B-symmetry deformations of the carbon backbone with frequencies in the range 1600-1700 cm$^{-1}$ (0.20-0.21 eV), and are responsible for the largest inter-state couplings (Table 3).

It is noteworthy that the largest HT intensities are found for two bright states S12 and S13. Their transition dipoles acquire a linear dependence (HT term) because the two states are coupled. However, when such HT terms are used in FCHT|VG, the effect is not a redistribution of the intensities between the two states (as predicted by LVC), but an overall spurious increase of the intensity of both states by a factor 3-4. This formally-wrong prediction usually introduces no problem when FCHT|VG is applied to very weak transitions, according to the spirit of the original HT theory. On the contrary, our results on [6]helicene show that it can introduce large artefacts if it is applied indiscriminately to weak and strong transitions. This feature strongly reduces the applicability of HT theory for systems characterized by a dense manifold of coupled states

### 3.2.2 Assignment of the 3.5-3.6 eV band.

We now turn to analyse the origin of the band at ∼3.5-3.6 eV. It is related to S2, because it disappears if S2 state is removed from the LVC model or if S2/S3 couplings are switched off (Figure S19 of the SI). However, this band is lower in energy than any S2 vibronic state (∼0.04 eV, by comparing panels (a) and (b) of Figure 2). This new vibronic state combines S2 and S3 contributions, and this is the reason why it can be predicted by LVC and not by FCHT|VG.

This explanation can be supported in different ways. First, with a "relaxation" calculation with MCTDH we can compute the lowest-energy vibronic state and, turning on or off the inter-state S2/S3 coupling we can investigate its effect. When the coupling is active, the energy of the lowest vibronic state is 0.07 eV lower than for the case it is switched off (Table S5 of the SI). This value is in line with the gap (∼0.04 eV) observed in Figure 2 between the lowest-energy band in the LVC spectrum (panel b) and lowest LVC band (panel a). The increased stability of the lowest vibronic state is connected with the existence of a double-well profile on the second adiabatic state due to the S2/S3 coupling (Figure S20 in the SI). A more direct confirmation can be obtained recomputing the spectrum in a TI framework, i.e. from the sum of the contributions of the vibronic eigenstates of the LVC model. In fact, with this approach each eigenstate (i.e. each band) can be analysed in terms of the contributions of the states of the basis set. Unfortunately, a TI calculation is only viable for systems with

**Table 2:** HT contributions of the most relevant $B$ symmetry vibrational normal modes to the absorption intensities (in atomic units) of S2 and S10-S13 states. The sum of the contributions of the normal modes here displayed and the total HT intensity ($I^{HT}_{ABS}$) are shown, together with the fraction of the total that these modes represent.

| | ABS Intensity (a.u.) | | | | |
|---|---|---|---|---|---|
| Mode | S2(A) | S10(A) | S11 (B) | S12 (A) | S13 (B) |
| v97 | 0.87 | 0.40 | 0.36 | 0.02 | 0.04 |
| v99 | 1.12 | 0.10 | 0.30 | 0.03 | 0.26 |
| v102 | 0.20 | 0.01 | 0.05 | 0.73 | 1.08 |
| v104 | 0.23 | 0.34 | 0.38 | 2.80 | 4.02 |
| Sum | 2.42 | 0.85 | 1.09 | 3.58 | 5.40 |
| Total $I^{HT}_{ABS}$ | 3.31 | 2.37 | 4.56 | 6.46 | 8.75 |
| Fraction of $I^{HT}_{ABS}$ | 0.73 | 0.36 | 0.24 | 0.55 | 0.62 |

few degrees of freedom. Therefore, we designed a 3-states, four-modes reduced model, only considering S1-S3 and the two normal modes with largest couplings of each symmetry (v85($A$), v88($A$), v97($B$) and v99($B$)). Results for ABS are shown in Figure 3 and compared with FC|VG and FCHT|VG predictions for the same reduced model (ECD analysis is in Figure S23 of the SI). The lowest-energy LVC transition is intense for both ABS and ECD and is responsible for the band at ∼3.5-3.6 eV in the experiment. It is more stable than any S2 level because of its mixed character involving both S2 and S3: it has a contribution 40% from the lowest (0) S3 level which is coupled to S2 states with 1 quantum number on the two B modes v97 and v99, i.e. those modes responsible for the S2/S3 coupling. The peaks at 3.8 and 4.0 eV also have a mixed nature which determine their energy: they are made up by S2 states with an odd number of quanta on the two B modes and few S3 states, namely 0 and other ones with an even number of quanta on the B modes. Finally the band at ∼4.1 eV includes contributions from progressions along the A mode v85. Differently from LVC, FC|VG spectrum predicts a non-vanishing intensity only for S3 vibrational states; in particular it is made up by the 0 band and a progression along mode v85. FCHT|VG does include the effect of S2/S3 coupling. However, since it assumes that the vibrational states do neither mix nor change their energy, the result is even worse than for FC|VG. In fact FCHT|VG predicts a significant enhancement of the S2 intensity for vibrationally-excited states with 1 quantum on modes v97 or v99. These states fall practically at the same energy of the S3 progression along v85, resulting in an erroneous and remarkable increase of the intensity in the region of S3.

**Table 3:** Interstate couplings ($\boldsymbol{\lambda}_{ij}(\alpha)$, in eV) between states $i$ and $j$, S2/S3, S10/S11 and S12/S13 states due to the normal coordinates ($\alpha$) with largest transition dipole derivatives. The total coupling (i.e. the norm of the vector $\boldsymbol{\lambda}_{ij}$)) for each pair of states is also given.

| Normal Coordinate | S2/S3 | S10/S11 | S12/S13 |
|---|---|---|---|
| v97 | 0.121 | 0.033 | 0.000 |
| v99 | 0.182 | 0.005 | -0.002 |
| v102 | -0.026 | -0.010 | -0.026 |
| v104 | -0.029 | 0.020 | -0.048 |
| Total Coupling (eV) | 0.263 | 0.066 | 0.071 |

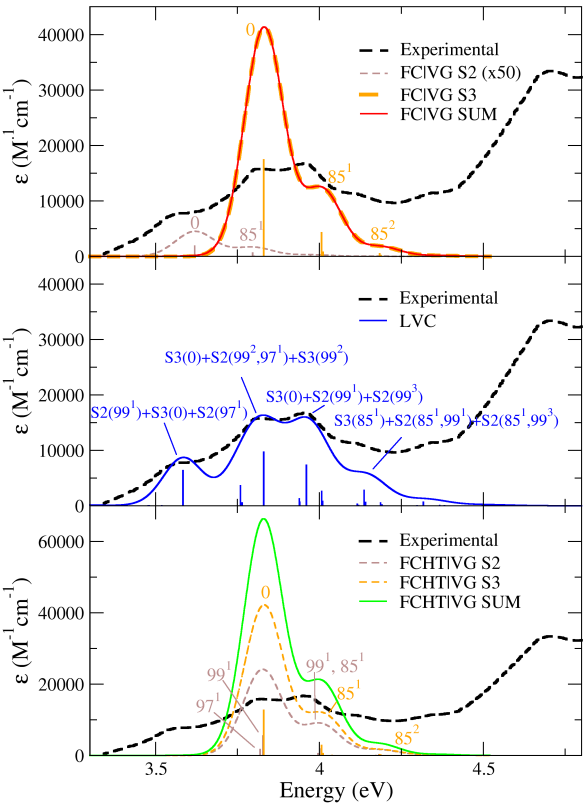


**Figure 3:** Experimental ABS spectra of ($M$)-[6]helicene compared with FC|VG (top), LVC (center, auto only) and FCHT|VG (bottom) predictions for a reduced model with states S1-S3 and the four normal modes with largest couplings: v85(A), v88(A), v97(B) and v99(B). Assignments are reported for the most intense stick transitions in terms of the adiabatic vibronic states. LVC eigenstates are made up by many contributions and only those corresponding to the three largest weights (in decreasing order) are given. Notice the larger $y$−scale for FCHT|VG, and that FC|VG S2 spectrum was amplified by a factor of 50. Calculated spectra were redshifted by 0.28 eV, a value larger than in Figure 2 to account for the zero point energies of the missing modes, and scaled by a factor of 0.7. All stick transitions were convoluted with a wider Gaussian of HWHM=0.07 eV to phenomenologically account for the missing coordinates.

### 3.2.3 The onset of the spectrum at ∼ 3.0 eV

We now focus on the onset of the experimental spectra at ∼3 eV that is too weak to be observed with the $y$-scale of the previous figures. This portion of the spectrum was already investigated at FCHT level in ref.[48] with CAM-B3LYP/TZVP calculations, concluding that it is strongly affected by the intensity-borrowing from higher-energy states. Here we evaluate the performance of LVC model in this region, comparing LVC, FC|VG and FCHT|VG spectra in Figure 4. Before entering in the discussion, we notice that according to our level of calculation, S1 is too close in energy to S2 and S3. In fact Figure S25 shows that, according to all vibronic models, the S1 contribution is overwhelmed by the onset of the S2/S3 coupled signal (giving rise to the peak at 3.5-3.6 eV), which erases the vibronic bands actually observed in the experiment. Therefore results presented in Figure 4 have been obtained applying to S1 vertical excitation a relative red-shift by 0.27 eV with respect to S2 and S3.

Both FCHT|VG and LVC nicely reproduce the spectra and attribute the main bands to a progression along mode v85 (and also a weaker one along v88). FC|VG performs very poorly (most of all for ECD) confirming that the spectral shape in this region is dominated by the effect of inter-state couplings. More in detail, FCHT|VG provides a perfect agreement for the first two bands of ABS. However, it predicts a monosignated negative ECD, while in the experiment the lowest-energy experimental band is weak but positive. LVC improves over FCHT|VG by successfully reproducing the bisignated ECD shape, although the computed band at ∼ 3.0 eV is too broad. One can notice that the LVC ABS band at ∼ 3.20 eV lacks some intensity with respect to FCHT|VG. In Figure S26 we show that this inaccuracy is not corrected by including the effect of the cross-terms in Eq.5; it may be connected to the lack of the contribution of some weakly-involved modes, considered in VG (120 modes) but not in LVC (63 modes). However, it should be noticed that, part of the apparent intensity of this band in the experiment could actually be due to the fact that it almost coalesces with the onset of the S2/S3 coupled band peaked at ∼3.5-3.6 eV. In the computations, this effect is not observed because such band is narrower and therefore rises at higher energies. We should further highlight that, by applying a relative red-shift to $S_1$ (by ∼ 0.27 eV), we made an approximation, which in LVC calculations may have less innocent implications than in VG model. In fact LVC couplings and energy gaps are not anymore fully coherent and this may, in principle, lead to a distortion of the adiabatic PESs and/or an alteration of the affect of the couplings on the transition intensities. In summary, it is not easy to establish which between LVC and FCHT|VG performs better for the relative intensity of the band at ∼ 3.20 eV.

Computation of the spectrum in this frequency region with the same three-states four-modes LVC TI model adopted for Figure 3 leads to a reasonable agreement with the experiment (see Figure S24 the SI). Analysis of the S2 and S3 contributions to the lowest two bands (those at ∼ 3.05 and 3.2 eV in Figure 4 indicates that they are minimal < 0.1% (Table S8). The weak-coupling assumption of the HT theory is therefore fulfilled and this explains why in this energy-region the FCHT approach is successful. We can conclude that in this energy region FCHT|VG and LVC performs in a similar way and that at least part of the residual discrepancy of the computed spectral shapes with respect to the experiment is due to inaccuracies in the computed energy gaps between the three lowest-energy states.

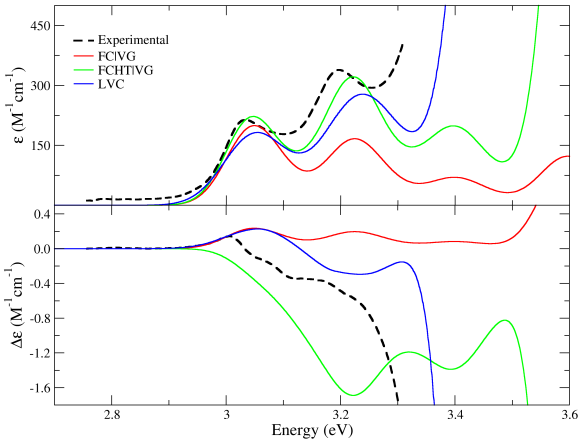


**Figure 4:** FC|VG, FCHT|VG and LVC ABS (top) and ECD (bottom) spectra of ($M$)-[6]helicene in the region 2.8-3.6 eV computed with M062X functional (for LVC, 63Q, 14 states, autocorrelation terms only). S2 and S3 position was blueshifted by 0.27 eV to correct the error on the excitation energies, and the overall spectra were redshifted by 0.48 eV, and scaled by a factor of 0.7. All stick transitions were convoluted with a Gaussian of HWHM=0.05 eV (0.06 eV for LVC, to include the effect of the missing coordinates).

## 3.3 Accuracy of the electronic calculations and LVC models with other functionals

LVC model allowed us a rather complete description of the vibronic bands and their different origin, and the assignment of the experimental bands. Therefore we can now also use these results to post-analyse the accuracy of the adopted M06-2X/6-31G(d) electronic level of theory. As far as S1 is concerned, as just discussed, we can conclude that is blue-shifted by ∼ 0.48 eV. Focusing on the other regions of the spectrum, even the simple electronic spectrum in Figure 1 indicates that the computational error on the position of bands is different in the regions 3.3-4.4 eV and > 4.4 eV. Since our LVC computations predict that the main features of the computed spectra in each of the two regions do not significantly depend on the states falling in the other region (see Figure S27), in Figure 5 we analyse separately the two different regions. FCHT|VG data are not reported

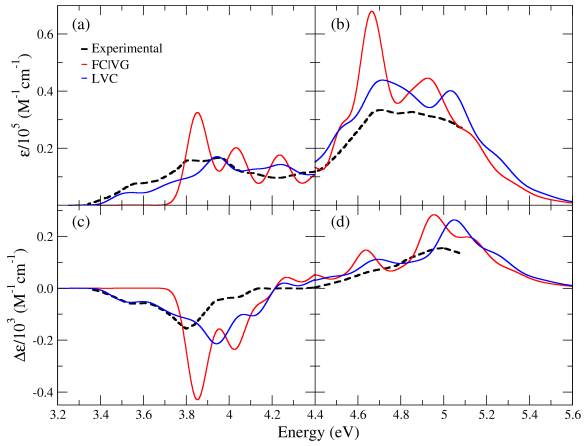


**Figure 5:** Experimental and calculated ABS (top) and ECD (bottom) spectra of (*M*)-[6]helicene in the regions (in eV) 3.2-4.4 (a,c), and 4.4-5.6 (b,d). All spectra were computed with M062X functional (for LVC, 63Q, 14 states, auto-correlation terms only). The spectra on panels a,c (b,d) were redshifted by 0.21 (0.58) eV, and scaled by a factor of 0.7. All stick transitions were convoluted with a Gaussian of HWHM=0.05 eV.

since, as documented above, they exhibit large artefacts. Figure 5 suggests that at M06-2X/6-31G* level of theory, the computed spectrum it is blue-shifted by $\sim$ 0.21 eV in the region 3.3-4.4 eV and by $\sim$0.58 eV above 4.4 eV.

Panels (b) and (d) of Figure 5 emphasize that also in the high-energy range the LVC spectral shapes are in good agreement with the experimental results, and improve over FC|VG, although only moderately. More specifically, especially for absorption, LVC bands are broader and less structured than FC|VG ones being more similar to the experimental ones. As already discussed, in the 3.3-4.4 eV range, LVC successfully predicts three bands at 3.5-3.6, 3.8 and 4.0 eV for both ABS and ECD, whereas FC|VG completely misses the band at 3.5-3.6 eV. The most significant inaccuracy of the LVC predictions concerns the ECD intensity at 4.0 eV, which is strongly overestimated. This happens because, in the region $\sim$ 3.6-4.0 eV, LVC predicts very similar shapes for ABS and ECD (apart from the sign), while experiments show a remarkable difference for the band at 4.0 eV. This discrepancy can have many causes, but surely inaccuracies in the electronic calculations have a significant impact. The possible effects of the level of electronic theory are analysed in Figure 6 comparing the predictions of LVC models parametrized with respect to M06-2X (previous Figures), B3LYP/GD3BJ and CAM-B3LYP/GD3BJ, with the 6-31G(d) basis set. It is noteworthy that B3LYP/GD3BJ provides spectral shapes in very good agreement with experiment (perfect for ECD) in the region 3.7-4.2 eV, and also slightly improves the predictions in the region 4.4-5.6 eV. However, the band at $\sim$3.5-3.6 eV appears slightly red-shifted and, most of all, the sign inversion of the ECD at $\sim$3.0 eV is not reproduced (Figure S30). As far as the position of the spectrum is concerned B3LYP/GD3BJ red-shifts it by $\sim$ 0.3 eV with respect to M062X. Finally, a LVC parametrized with CAM-B3LYP/GD3BJ delivers spectra very similar to M06X (Figure 6, considering both the shape and the position). On the balance these results confirm that the residual discrepancies with experiment might derive in large part from inaccuracies of the electronic calculations.

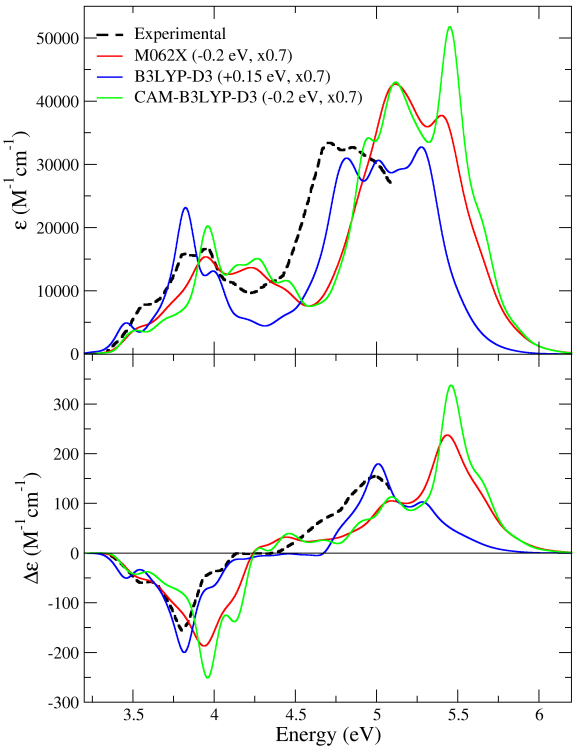


**Figure 6:** Comparison of (*M*)-[6]helicene ABS (top) and ECD (bottom) LVC spectra obtained from diabatization of the excited states calculated at the M062X/6-31G(d) (63Q, 14 states), B3LYP/GD3BJ/6-31G(d) (65Q, 18 states) and CAM-B3LYP/GD3BJ/6-31G(d) (63Q, 14 states) levels of theory. Computed spectra were shifted (0.2 eV to the red for M062X and CAM-B3LYP and 0.1 eV to the blue for B3LYP) and scaled by a factor of 0.7. All stick transitions were convoluted with a Gaussian of HWHM = 0.05 eV.

# 4 Conclusions

In this contribution we have shown that, thanks to the effective methodology recently developed to parametrize LVC models for several coupled states from TD-DFT calculations,[18] and to the capabilities of ML-MCTDH QD propagations,[39] it is nowadays possible to get a reliable description of the nonadiabatic effects of the absorption and ECD spectra of [6]helicene in a range of $\sim$ 2 eV, including all the couplings among the lowest 14 electronic states (18 for B3LYP/GD3BJ) and the contributions of all relevant normal coordinates (>60). These effects are particularly strong between S2 and S3, creating a double-well in the lower adiabatic PES

and new vibronic bands, which mix S2 and S3 contributions and cannot be described with perturbative approaches like HT theory. The proposed computational protocol is effective enough to represent a feasible root to describe vibronic effects in the optical and chiroptical properties of more extended helicene-like compounds and, more in general, of large $\pi$-conjugated systems. Beside its application to steady-state spectroscopy, this protocol will also help to study the QD of internal conversions in these systems (an example is in Figure S31 of the SI). HT theory was originally developed to describe intensity borrowing of weakly-coupled weak transitions. Our results clearly document that an indiscriminate use of FCHT approach, extended also to bright states with strong couplings, can lead to huge artefacts, such as an unphysical growing of the intensity, making the FCHT predictions unreliable. The relevance of this conclusion goes beyond the specific case of [6]helicene, rising a general warning to the use of HT theory to describe vibronic contributions in systems with many close electronic states. For these systems, non-perturbative coupled approaches like LVC should be the method of choice. If simpler adiabatic calculations are performed for a first qualitative analysis of the spectrum, FC approximation should be preferred to FCHT since, at least, it guarantees the correct reproduction of the total intensity.

## Supporting Information

Theory and computation details. Convergence tests. Comparison of LVC spectra (setting the couplings to zero) and FC|VG spectra for each state. Additional analysis on the S1 and S2-S3 regions of the spectra. Sketches of the most relevant normal modes. Further details on the origin of the 3.5-3.6 eV band. Assignment of vibronic states using a time-independent LVC model. LVC spectra parametrized with different functionals. Example of population dynamics.

## Acknowledgements

DA acknowledges Fundación Ramón Areces (Spain) for funding his postdoctoral stay at ICCOM-CNR Pisa. The authors thank Dr Yanli Liu (Ludong University, China) for useful discussions.

# References


(1) Hazra, A.; Chang, H. H.; Nooijen, M. First principles simulation of the UV absorption spectrum of ethylene using the vertical Franck-Condon approach. *J. Chem. Phys.* **2004**, *121*, 2125–2136.

(2) Dierksen, M.; Grimme, S. An efficient approach for the calculation of Franck–Condon integrals of large molecules. *J. Chem. Phys.* **2005**, *122*, 244101.

(3) Santoro, F.; Improta, R.; Lami, A.; Bloino, J.; Barone, V. Effective method to compute Franck-Condon integrals for optical spectra of large molecules in solution. *J. Chem. Phys.* **2007**, *126*, 084509.

(4) Santoro, F.; Lami, A.; Improta, R.; Bloino, J.; Barone, V. Effective method for the computation of optical spectra of large molecules at finite temperature including the Duschinsky and Herzberg–Teller effect: The Qx band of porphyrin as a case study. *J. Chem. Phys.* **2008**, *128*, 224311.

(5) Jankowiak, H.-C.; Stuber, J. L.; Berger, R. Vibronic transitions in large molecular systems: Rigorous prescreening conditions for Franck-Condon factors. *J. Chem. Phys.* **2007**, *127*, 234101.

(6) Bloino, J.; Biczysko, M.; Santoro, F.; Barone, V. General Approach to Compute Vibrationally Resolved One-Photon Electronic Spectra. *J. Chem. Theory Comput.* **2010**, *6*, 1256–1274.

(7) Ianconescu, R.; Pollak, E. Photoinduced Cooling of Polyatomic Molecules in an Electronically Excited State in the Presence of Dushinskii Rotations. *J. Phys. Chem. A* **2004**, *108*, 7778–7784.

(8) Peng, Q.; Niu, Y.; Deng, C.; Shuai, Z. Vibration correlation function formalism of radiative and non-radiative rates for complex molecules. *Chem. Phys.* **2010**, *370*, 215–222.

(9) Borrelli, R.; Capobianco, A.; Peluso, A. Generating Function Approach to the Calculation of Spectral Band Shapes of Free-Base Chlorin Including Duschinsky and Herzberg-Teller Effects. *J. Phys. Chem. A* **2012**, *116*, 9934–9940.

(10) Huh, J.; Berger, R. Coherent state-based generating function approach for Franck-Condon transitions and beyond. *J. Phys.: Conf. Ser.* **2012**, *380*, 012019.

(11) Baiardi, A.; Bloino, J.; Barone, V. General Time Dependent Approach to Vibronic Spectroscopy Including Franck-Condon, Herzberg-Teller, and Duschinsky Effects. *J. Chem. Theory Comput.* **2013**, *9*, 4097–4115.

(12) Avila Ferrer, F. J.; Cerezo, J.; Soto, J.; Improta, R.; Santoro, F. First-principle computation of absorption and fluorescence spectra in solution accounting for vibronic structure, temperature effects and solvent inhomogenous broadening. *Comput. Theoret. Chem.* **2014**, *1040–1041*, 328–337.

(13) Beck, M. H.; Jäckle, A.; Worth, G. A.; Meyer, H.-D. The multiconfiguration time-dependent Hartree method: A highly efficient algorithm for propagating wavepackets. *Phys. Rep.* **2000**, *324*, 1–105.

(14) Meyer, F., H.-D.and Gatti, Worth, G. A., Eds. *Multidimensional Quantum Dynamics: MCTDH Theory and Applications*; Wiley-VCH: Weinheim, 2009.

(15) Wang, H.; Thoss, M. Multilayer formulation of the multiconfiguration time-dependent Hartree theory. *J. Chem. Phys.* **2003**, *119*, 1289–1299.

(16) Manthe, U. Layered discrete variable representations and their application within the multiconfigurational time-dependent Hartree approach. *J. Chem. Phys.* **2009**, *130*, 054109.

(17) Vendrell, O.; Meyer, H.-D. Multilayer multiconfiguration time-dependent Hartree method: Implementation and applications to a Henon-Heiles Hamiltonian and to pyrazine. *J. Chem. Phys.* **2011**, *134*, 044135.

(18) Yaghoubi Jouybari, M.; Liu, Y.; Improta, R.; Santoro, F. The Ultrafast Dynamics of the Two Lowest Bright Excited States of Cytosine and 1-Methyl-Cytosine: A Quantum Dynamical Study. *J. Chem. Theory Comput.* **2020**, *16*, 5792–5808.

(19) Köppel, H.; Domcke, W.; Cederbaum, L. S. *Advances in Chemical Physics*; John Wiley & Sons, Ltd, 1984; pp 59–246.

(20) Köppel, H.; Domcke, W.; Cederbaum, L. The Multi-mode vibronic-coupling approach . Conical Intersections, Electronic Structure, Dynamics and Spectroscopy. 2004; pp 323–368.

(21) Shen, Y.; Chen, C.-F. Helicenes: Synthesis and Applications. *Chemical Reviews* **2012**, *112*, 1463–1535, PMID: 22017405.

(22) Gingras, M. One hundred years of helicene chemistry. Part 1: non-stereoselective syntheses of carbohelicenes. *Chem. Soc. Rev.* **2013**, *42*, 968–1006.

(23) Schuster, N. J.; Hernández Sánchez, R.; Bukharina, D.; Kotov, N. A.; Berova, N.; Ng, F.; Steigerwald, M. L.; Nuckolls, C. A Helicene Nanoribbon with Greatly Amplified Chirality. *Journal of the American Chemical Society* **2018**, *140*, 6235–6239, PMID: 29757639.

(24) Xiao, X.; Pedersen, S. K.; Aranda, D.; Yang, J.; Wiscons, R. A.; Pittelkow, M.; Steigerwald, M. L.; Santoro, F.; Schuster, N. J.; Nuckolls, C. Chirality Amplified: Long, Discrete Helicene Nanoribbons. *Journal of the American Chemical Society* **2020**, *10.1021/jacs.0c11260*.

(25) Autschbach, J. Computing chiroptical properties with first-principles theoretical methods: Background and illustrative examples. *Chirality* **2009**, *21*, E116–E152.

(26) Autschbach, J. In *Comprehensive Chiroptical Spectroscopy, vol I*; Berova, N., Polavarapu, P. L., Nakanishi, K., Woody, R. W., Eds.; Wiley, 2012; pp 593–642.

(27) Harada, N.; Chen, S.-M. L.; Nakanishi, K. Quantitative definition of exciton chirality and the distant effect in the exciton chirality method. *J. Am. Chem. Soc.* **1975**, *97*, 5345–5352.

(28) Harada, N.; Nakanishi, K.; Berova, N. In *Comprehensive Chiroptical Spectroscopy*; Berova, N., Polavarapu, P. L., Nakanishi, K., Woody, R. W., Eds.; Wiley, 2012; pp 115–166.

(29) Swathi, K.; Sissa, C.; Painelli, A.; George Thomas, K. Supramolecular chirality: a caveat in assigning the handedness of chiral aggregates. *Chem. Commun.* **2020**, *56*, 8281–8284.

(30) Herzberg, G.; Teller, E. Fluctuation structure of electron transfer in multiatomic molecules. *Z. Phys. Chem. B* **1933**, *21*, 410.

(31) Liu, Y.; Cerezo, J.; Santoro, F.; Rizzo, A.; Lin, N.; Zhao, X. Theoretical investigation of the broad one-photon absorption line-shape of a flexible symmetric carbazole derivative. *Phys. Chem. Chem. Phys.* **2016**, *18*, 22889–22905.

(32) Padula, D.; Lahoz, I. R.; Díaz, C.; Hernández, F. E.; Di Bari, L.; Rizzo, A.; Santoro, F.; Cid, M. M. A Combined Experimental–Computational Investigation to Uncover the Puzzling (Chiro-)optical Response of Pyridocyclophanes: One- and Two-Photon Spectra. *Chemistry – A European Journal* **2015**, *21*, 12136–12147.

(33) Ozcelik, A. et al. Distinct helical molecular orbitals through conformational lock. **2020**,

(34) Avila Ferrer, F. J.; Santoro, F. Comparison of vertical and adiabatic harmonic approaches for the calculation of the vibrational structure of electronic spectra. *Phys. Chem. Chem. Phys.* **2012**, *14*, 13549–13563.

(35) Transition dipole derivatives can be obtained directly from quantum-chemistry codes and in the Supporting Information we test that results computed in this way or obtaining the derivatives from the LVC model are extremely similar. However we use the latter for a full coherence of our data.

(36) Grimme, S.; Ehrlich, S.; Goerigk, L. Effect of the damping function in dispersion corrected density functional theory. *Journal of computational chemistry* **2011**, *32*, 1456–1465.

(37) Nakai, Y.; Mori, T.; Inoue, Y. Theoretical and experimental studies on circular dichroism of carbo [n] helicenes. *The Journal of Physical Chemistry A* **2012**, *116*, 7372–7385.

(38) Frisch, M. J. et al. Gaussian˜16 Revision B.01. 2016; Gaussian Inc. Wallingford CT.

(39) Worth, G. A.; Giri, K.; Richings, G. W.; Beck, M. H.; Jäckle, A.; Meyer, H.-D. The QUANTICS Package, Version 1.1, (2015), University of Birmingham, Birmingham, U.K.

(40) Worth, G. Quantics: A general purpose package for Quantum molecular dynamics simulations. *Computer Physics Communications* **2020**, *248*, 107040.

(41) Santoro, F.; Cerezo, J. $\mathcal{FC}classes3$, a code for vibronic calculations. Available upon request. 2019.

(42) Abbate, S. et al. Helical sense-responsive and substituent-sensitive features in vibrational and electronic circular dichroism, in circularly polarized luminescence, and in Raman spectra of some simple optically active hexahelicenes. *The Journal of Physical Chemistry C* **2014**, *118*, 1682–1695.

(43) Weigang Jr, O. E. Vibrational Structuring in Optical Activity. II."Forbidden"Character in Circular Dichroism. *The Journal of Chemical Physics* **1965**, *43*, 3609–3618.

(44) Lin, N.; Luo, Y.; Santoro, F.; Zhao, X.; Rizzo, A. Vibronically-induced change in the chiral response of molecules revealed by electronic circular dichroism spectroscopy. *Chemical Physics Letters* **2008**, *464*, 144 – 149.

(45) Pescitelli, G.; Barone, V.; Di Bari, L.; Rizzo, A.; Santoro, F. Vibronic Coupling Dominates the Electronic Circular Dichroism of the Benzene Chromophore 1Lb band. *The Journal of Organic Chemistry* **2013**, *78*, 7398–7405, PMID: 23834013.

(46) Liu, Y.; Cerezo, J.; Mazzeo, G.; Lin, N.; Zhao, X.; Longhi, G.; Abbate, S.; Santoro, F. Vibronic Coupling Explains the Different Shape of Electronic Circular Dichroism and of Circularly Polarized

Luminescence Spectra of Hexahelicenes. *Journal of Chemical Theory and Computation* **2016**, *12*, 2799–2819, PMID: 27120334.

(47) Nooijen, M. Investigation of Herzberg–Teller Franck–Condon approaches and classical simulations to include effects due to vibronic coupling in circular dichroism spectra: The case of dimethyloxirane continued. *International journal of quantum chemistry* **2006**, *106*, 2489–2510.

(48) Liu, Y.; Cerezo, J.; Mazzeo, G.; Lin, N.; Zhao, X.; Longhi, G.; Abbate, S.; Santoro, F. Vibronic coupling explains the different shape of electronic circular dichroism and of circularly polarized luminescence spectra of hexahelicenes. *Journal of chemical theory and computation* **2016**, *12*, 2799–2819.

## Graphical TOC Entry

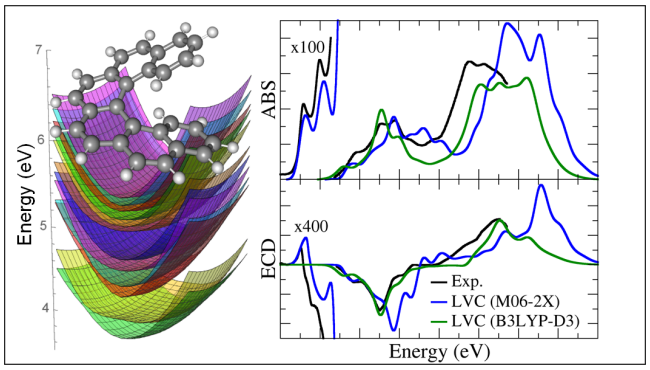


(*M*)-[6]helicene potential energy surfaces and ABS/ECD spectra.